Computer Methods in Biomechanics and Biomedical Engineering

Publication details, including instructions for authors and subscription information:
http://www.tandfonline.com/loi/gcmb20

Fluid-structure interaction analysis of the left coronary artery with variable angulation

Jingliang Dong[a], Zhonghua Sun[b], Kiao Inthavong[a] & Jiyuan Tu[a]

[a] School of Aerospace, Mechanical & Manufacturing Engineering, Platform Technologies Research Institute (PTRI), RMIT University, PO Box 71, Bundoora, VIC 3083, Australia

[b] Discipline of Medical Imaging, Department of Imaging and Applied Physics, Curtin University, GPO Box U1987, Perth, WA 6845, Australia

Published online: 05 Jun 2014.

To cite this article: Jingliang Dong, Zhonghua Sun, Kiao Inthavong & Jiyuan Tu (2014): Fluid-structure interaction analysis of the left coronary artery with variable angulation, Computer Methods in Biomechanics and Biomedical Engineering, DOI: 10.1080/10255842.2014.921682

To link to this article: http://dx.doi.org/10.1080/10255842.2014.921682

Computer Methods in Biomechanics and Biomedical Engineering, 2014
http://dx.doi.org/10.1080/10255842.2014.921682

Taylor & Francis
Taylor & Francis Group

Fluid–structure interaction analysis of the left coronary artery with variable angulation

Jingliang Dong[a], Zhonghua Sun[b], Kiao Inthavong[a] and Jiyuan Tu[a]*

[a]*School of Aerospace, Mechanical & Manufacturing Engineering, Platform Technologies Research Institute (PTRI), RMIT University, PO Box 71, Bundoora, VIC 3083, Australia;* [b]*Discipline of Medical Imaging, Department of Imaging and Applied Physics, Curtin University, GPO Box U1987, Perth, WA 6845, Australia*

(*Received 23 January 2014; accepted 2 May 2014*)

The aim of this study is to elucidate the correlation between coronary artery branch angulation, local mechanical and haemodynamic forces at the vicinity of bifurcation. Using a coupled fluid–structure interaction (FSI) modelling approach, five idealized left coronary artery models with various angles ranging from 70° to 110° were developed to investigate the influence of branch angulations. In addition, one CT image-based model was reconstructed to further demonstrate the medical application potential of the proposed FSI coupling method. The results show that the angulation strongly alters its mechanical stress distribution, and the instantaneous wall shear stress distributions are substantially moderated by the arterial wall compliance. As high tensile stress is hypothesized to cause stenosis, the left circumflex side bifurcation shoulder is indicated to induce atherosclerotic changes with a high tendency for wide-angled models.

Keywords: left coronary artery; branch angulation; fluid–structure interaction; arterial wall compliance; tensile stress; wall shear stress

1. Introduction

Coronary heart disease is a leading cause of death worldwide with 6.2 million deaths reported in 1990; this figure is estimated to nearly double by 2020 (World Health Organization 2002). It is primarily caused by atherosclerosis due to the formation, development and rupture of plaques (Ohayon et al. 2008). Plenty of evidence implicates the mechanical forces and intravascular haemodynamics that result from blood flow [e.g. high circumferential tensile stress and low wall shear stress (WSS)] and can chronically affect and regulate blood vessel structure (Caro et al. 1969; Malek et al. 1999; Slager et al. 2005). Atherosclerotic plaques typically occur in arterial regions that display complex geometry resulting in 'disturbed' blood flow behaviour (Ku et al. 1985; Cecchi et al. 2011). However, the complex aetiology of atherosclerosis is not fully understood due to unknown relationships between haemodynamics, mechanical factors and atherosclerotic changes of the arterial wall. Although WSS has been implicated in inducing endothelial wall cell responses (Stone et al. 2007), identifying WSS from flow patterns and mechanical forces *in vivo* is difficult (Vennemann et al. 2007).

Image-based computational fluid dynamics studies can provide more detailed flow patterns such as WSS distribution in arterial vessels that cannot be revealed directly from medical imaging. Flow indicators such as low mean WSS (Caro et al. 1971; Soulis et al. 2006; Gijsen et al. 2007; Cecchi et al. 2011) and oscillatory shear index (OSI; Ku et al. 1985; Dong, Inthavong, Tu 2013; Dong, Wong, Tu 2013) are widely used to identify and correlate disturbed flow with atherosclerotic disease location. However, these studies are largely based on rigid wall assumptions neglecting the elasticity of the arterial wall.

The fluid–structure interaction (FSI) approach simultaneously models blood flow (fluid) and arterial wall deformations (structure) and has received growing interest because of its potential impact in the medical field (Vigmostad et al. 2010; Heil and Hazel 2011). It has been implemented in modelling abdominal aorta (Scotti et al. 2005; Leung et al. 2006), carotid bifurcation (Karner et al. 1999; Tada and Tarbell 2005) and cerebral aneurysm (Torii, Oshima et al. 2009; Tezduyar et al. 2011).

Torii, Wood et al. (2009) studied the effects of wall compliance on a patient-specific right coronary artery with a severe stenosis and found noticeable differences in the instantaneous WSS produced by the FSI and rigid wall models. Huo et al. (2009) investigated the effect of vessel compliance on flow patterns in porcine epicardial right coronary artery through *in vivo* measurement and FSI analysis. They found that the time-averaged WSS gradient value predicted by the compliant FSI model was smaller than those found for rigid bifurcations. To improve the stress–strain prediction accuracy, cyclic bending and anisotropic vessel properties were added to FSI coronary plaque models by Tang et al. (2009).

In summary, the majority of the previous numerical studies often neglected either the vessel compliance or the

*Corresponding author. Email: jiyuan.tu@rmit.edu.au

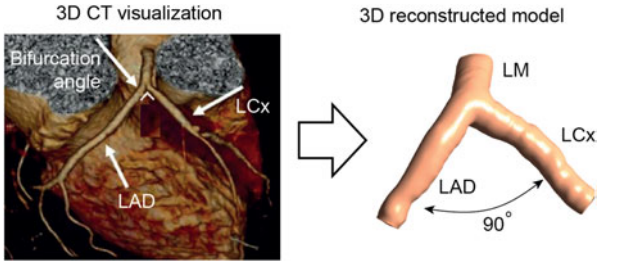

Figure 1. 3D CT visualization and reconstruction of the image-based model.

bifurcation. Despite Malve et al. (2012) performed FSI and rigid wall modellings on a healthy left coronary artery bifurcation reconstructed from CT scans, the cross-sectional area was simplified into circular shape. Therefore, the non-uniform surface nature due to local anatomical variations was not taken into account. Tang et al. (2009) developed a complex model of a stenotic vessel segment, but the effect of bifurcations was neglected.

This paper presents for the first time an FSI study of the correlation between coronary artery branch angulation, local mechanical and haemodynamic forces using anatomically accurate and idealized human coronary artery models. This study aims to elucidate the link between coronary artery angulation, coronary haemodynamics (OSI) and local mechanical forces (tensile stress) to enable a better understanding of the role of haemodynamics in atherosclerotic disease initiation and progression in the vicinity of bifurcations. To fulfil this research objective, FSI coupling was applied on one anatomically accurate human coronary artery model and five idealized models with different bifurcation angulations (θ) between its two main branches.

Table 1. Anatomical dimensions of the idealized model.

Length of LM	11.0 mm
Dia. of LM	4.0 mm
Dia. of LAD	3.4 mm
Dia. of LCx	3.0 mm
Rad. of curvature of LAD	42.8 mm
Rad. of curvature of LCx	39.3 mm
Angulation between LM and LAD	159°
Vessel wall thickness	0.4 mm

Note: LM, left main stem; LAD, left anterior descending; LCx, left circumflex.

2. Methods

2.1 Geometry reconstruction of arterial models

The anatomical replica model was reconstructed from multi-slice CT angiography of a left coronary segment conducted previously by Chaichana et al. (2011). Figure 1 shows the CT image-based model which exhibits an angle of 90° generated from CT images (voxel size of 0.6 × 0.6 × 0.6 mm^3) using Blender version 2.48 (Blender Institute, Amsterdam, The Netherlands). In addition, a set of idealized models were developed based on 19 post-mortem casts of normal human coronary artery trees (Nerem and Seed 1983), which averaged anatomical data for vessel diameter, length and curvature. An overview of the idealized model is shown in Figure 2, and its basic dimensions are listed in Table 1. To analyse the influence of bifurcation angulation (θ) on coronary artery haemodynamics, five idealized models were constructed with angles of 70°, 80°, 90°, 100° and 110°, respectively, which are in the physiological range reported by Girasis et al. (2010). To isolate the effect of a single geometric factor, the angle formed by left main stem (LM) and left anterior descending (LAD) was kept constant (Johnston and Kilpatrick 1997). Then, the angle variation was achieved through changing the orientation of left circumflex (LCx).

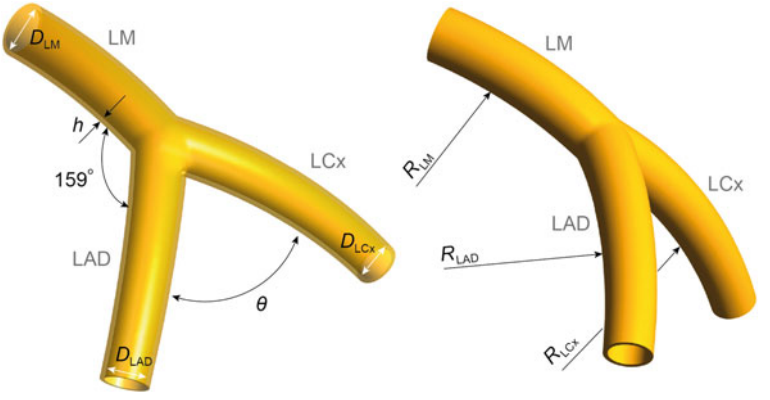

Figure 2. Geometry configuration of the idealized artery model. h indicates vessel wall thickness, D stands for vessel diameter and R for branch curvature.

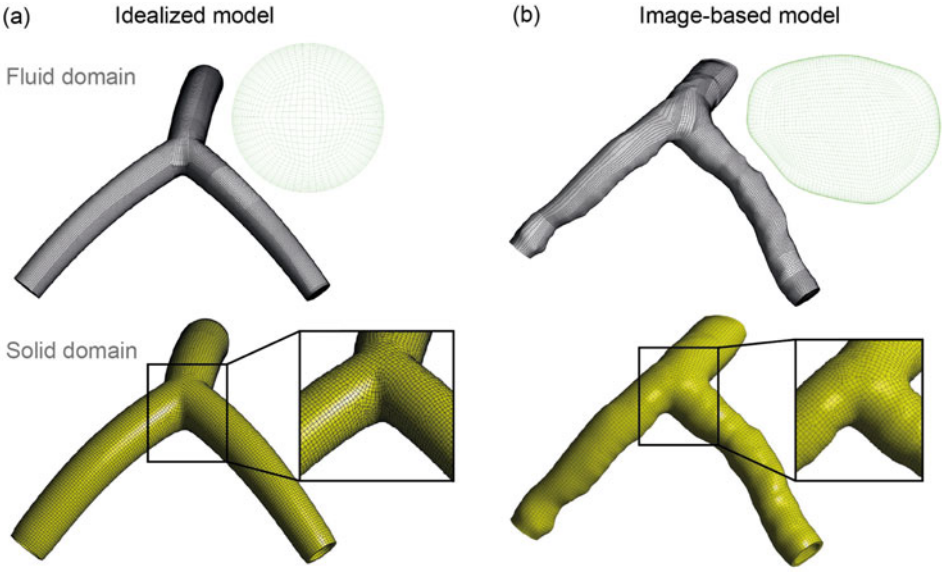

Figure 3. Structure mesh results of (a) idealized and (b) image-based models.

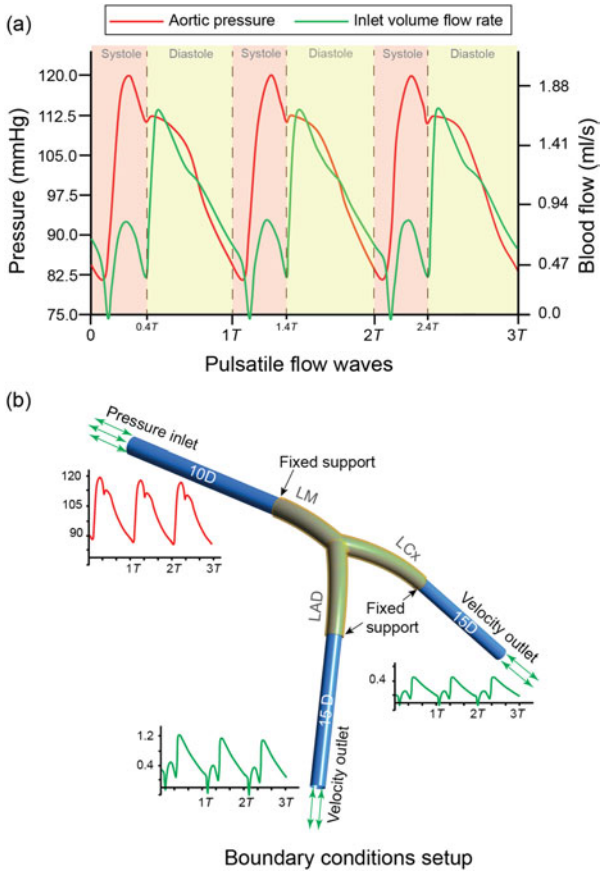

Figure 4. Pulsatile blood flow waves used in this study. *T* stands for one cardiac cycle.

2.2 Mesh generation and physiological boundary conditions

For each coronary artery model, both fluid and structural domains were meshed with hexahedral cells to minimize numerical diffusion and lower the number of elements. A near wall grid refinement was imposed on each model to provide better resolution for near wall quantities. Mesh results for fluid domain and structural domain of the image-based model and the idealized model ($\theta = 90°$) are shown in Figure 3. As it is difficult to obtain the outer wall boundary of the artery from CT images, the vessel wall was artificially constructed with a constant thickness $h = 0.4$ mm (Colombo et al. 2010). Although arterial wall is known to be a composite tissue including collagen fibres, its heterogeneous and anisotropic structure properties were simplified by adopting a nine parameter Mooney–Rivlin hyperelastic model (Koshiba et al. 2007) due to lack of *in vivo* data.

The inlet and outlet boundary conditions shown in Figure 4(a) are based on a physiological pulsatile flow rate and pressure at the aorta (Nichols and O'Rourke 2005), reconstructed using a Fourier series in Matlab (Math Works, Inc., Natick, MA, USA). This Fourier series was inputted into ANSYS CFX Command Language programming to define boundary conditions. The blood flow distribution in the bifurcation adopts the method of Boutsianis et al. (2004), where 71% is directed through LAD and 29% through LCx, and this is maintained unchanged through the entire cardiac cycle. Pulsatile aortic pressure was applied as an inlet boundary condition at the entrance of LM, and pulsatile velocity conditions were imposed on both the LAD and the LCx outlet boundaries (Figure 4(b)). As this study focuses on the local haemodynamic changes under different branch angulations, global coronary wall motion due to its

Table 2. Mesh independence study of the three different mesh refinements.

	Coarse Mesh	Fine Mesh	Finest Mesh
Number of elements	398,178	818,714	1,997,318
Average Δx (mm)	0.21	0.15	0.09
WSS at the apex (Pa)	2.02[a]	2.11[a]	2.14[a]
Difference percentage	5.61%	1.40%	—
Computational time (h)	13	21	35

[a]Values were extracted at the peak of diastole phase.

attachment to the moving myocardium is neglected to isolate the effects of wall compliance (Torii, Wood et al. 2009; Malve et al. 2012).

The blood was assumed to be Newtonian as the shear rate is large enough in coronary arteries (larger than 100 s^{-1}) to maintain a flow regime with nearly constant viscosity (Joshi et al. 2004; Gijsen et al. 2007). The density and viscosity of the blood are 1060 kg/m^3 and 0.0035 Pa s, respectively (Chaichana et al. 2012). The blood flow was treated as laminar and no-slip condition was applied at arterial walls. To eliminate the local fluid dynamic effects on the reconstructed fluid domain and ensure fully developed outlet flow conditions, a 10-diameter length inlet extension and 15-diameter length outlet extensions were added (Joshi et al. 2004).

Mesh independence was conducted on the idealized model ($\theta = 100°$) using three mesh sizes, and the peak diastole WSS values at the bifurcation apex were compared (Table 2). Comparing with the finest mesh, the coarse mesh has the largest value difference percentage (5.47%) costing the shortest computational time (13 h), while the fine mesh has a closer prediction performance with a value difference percentage of 1.09% under an acceptable computational time duration (21 h). Hence, fine mesh size (0.15 mm) was chosen to conduct the rest of the simulations from accuracy and efficiency points of view.

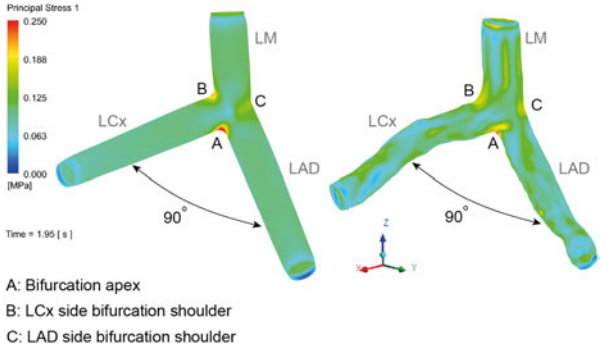

Figure 5. Comparison of first principal stress at peak systole ($t = 1.95$ s).

2.3 FSI simulation

The governing equations for the incompressible Navier–Stokes equations with arbitrary Lagrangian–Eulerian formulation are

$$\rho_b \frac{\partial u}{\partial t} + [((u - u_g)\cdot\nabla)u] = -\partial p + \mu\partial^2 u, \quad \nabla\cdot u = 0 \qquad (1)$$

with boundary conditions

$$p|_{intel} = p_{in}(t), \quad p|_{outlet} = p_{out}(t),$$

where u is the flow velocity, u_g is the mesh velocity, p is the pressure and μ and ρ_b stand for the blood viscosity and density, respectively.

The arterial wall motion is governed by

$$\rho_w v_{i,tt} = \sigma_{ij,j}, \quad i,j = 1,2,3;\ \text{sum over}\ j \qquad (2)$$

with boundary condition $\left|\sigma_{ij,j}\cdot n_j\right|_{\text{outer wall}} = 0$, where ρ_w is the vessel wall density, v is the displacement vector, $\Sigma$is the stress tensor and t denotes time.

The interaction between the fluid and structure is

$$\sigma^f_{ij}\dot{c}\, n_j|_\Gamma = \sigma^s_{ij}\dot{c}\, n_j|_\Gamma, \qquad (3)$$

where Γ represents the fluid–structure interface, and f and s stand for fluid part and structure part, respectively. The fully coupled FSI models were solved in commercial software packages ANSYS CFX and ANSYS Mechanical (ANSYS Inc., Canonsburg, PA, USA). ANSYS CFX is finite-volume-based software for fluid mechanics computations, and ANSYS Mechanical is finite-element-based software for structural mechanics analysis. FSI models are coupled and solved iteratively by these two packages within each time step by applying appropriate kinematic and dynamic conditions at the fluid–structure interface until the coupling system residual is less than a specified tolerance. For each coronary artery model, transient flow simulations over three cardiac cycles were performed, and results at the last cycle were used for mechanical and haemodynamic analysis.

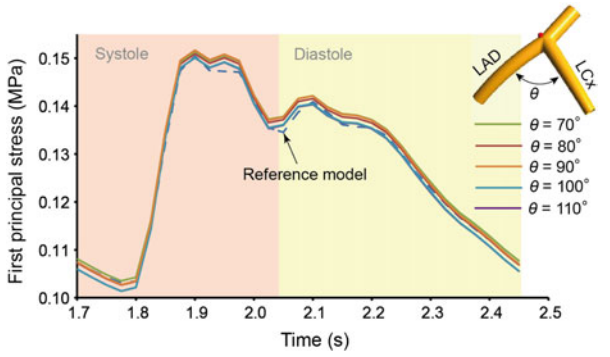

Figure 6. First principal stress profiles at the LAD side bifurcation shoulder.

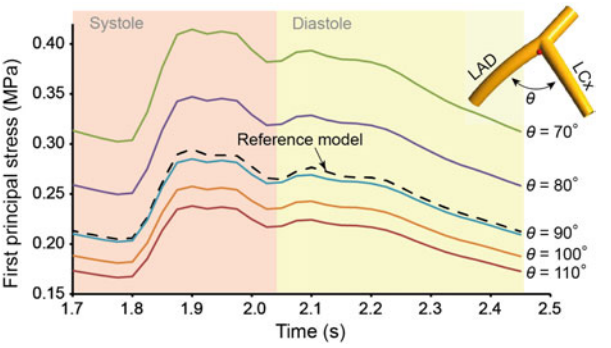

Figure 7. First principal stress profiles at the bifurcation apex.

3. Results

3.1 Mechanical results analysis

The first principal stress is used for stress distribution analysis, as it represents the maximum tensile stress included in the vessel wall due to the pulsatile loading of blood flow. Figure 5 shows the first principal stress distribution for the idealized ($\theta = 90°$) and the image-based models at peak systole phase. For the idealized model, high first principal stress value concentrates at the bifurcation area. The maximum value 0.28 MPa occurs at the bifurcation apex, followed by the bifurcation shoulders on LCx side (0.22 MPa) and LAD side (0.15 MPa), respectively. Similarly, the first principal stress distribution of the image-based model shows a similar result when compared with the idealized model ($\theta = 90°$). Due to its irregular vascular luminal shape, a fraction of left main stem (LM) luminal region experiences slightly stronger stress value than their corresponding locations on the idealized model.

To reveal the bifurcation angulation influence on stress distribution, the variations of the first principal stress at three reference locations indicated by three red dots, the LAD side bifurcation shoulder (Figure 6), the bifurcation apex (Figure 7) and the LCx side bifurcation shoulder (Figure 8) are reviewed. In general, the first principal stress shows a similar profile with aortic pressure, which demonstrates that the stress variation is mainly driven by the pulsatile aortic pressure. As the angle formed by LM and LAD is kept constant (159°), the stress variation profiles at the LAD side bifurcation shoulder are similar for all models (Figure 6), and hence, the bifurcation angle variation does not affect the stress distribution in this region.

Figure 7 shows the stress variation at the bifurcation apex, where the bifurcation angle is found to negatively correlate with the first principal stress value. For the narrowest idealized model ($\theta = 70°$), its maximum stress $\sigma_{max} = 0.41$ MPa occurs at the peak systole phase, while the widest idealized model ($\theta = 110°$) experiences $\sigma_{max} = 0.24$ MPa at the same time. This represents a value reduction of 41.5% due to bifurcation angle increase.

In contrast, a positive correlation is found between the first principal stress at the LCx side bifurcation shoulder and the bifurcation angle (Figure 8). As the angle increases, the maximum stress also increases 50% from 0.18 ($\theta = 70°$) to 0.27 MPa ($\theta = 110°$) at peak systole phase. Furthermore, the overall stress value at the bifurcation apex (Figure 6) is stronger than that of the LCx side shoulder (Figure 7) when $\theta < 100°$. When $\theta = 100°$, the stress difference between these two locations is significantly reduced. For the idealized model with $\theta = 110°$, the maximum stress occurs at the LCx side bifurcation shoulder ($\sigma_{max} = 0.27$ MPa) rather than the bifurcation apex ($\sigma_{max} = 0.24$ MPa).

The image-based model also displays a similar stress variation profile with the idealized model ($\theta = 90°$) both on the bifurcation apex and the LCx side bifurcation shoulder. Along with the results shown in Figure 5, it can be demonstrated that the idealized models are capable of representing key FSI results for further analysis.

3.2 Haemodynamic results analysis

The widely adopted flow indicator, WSS-based OSI, is used to evaluate the total shear stress exerted on the arterial wall (Figure 9). It can be regarded as the fraction of angle and magnitude change between the instantaneous

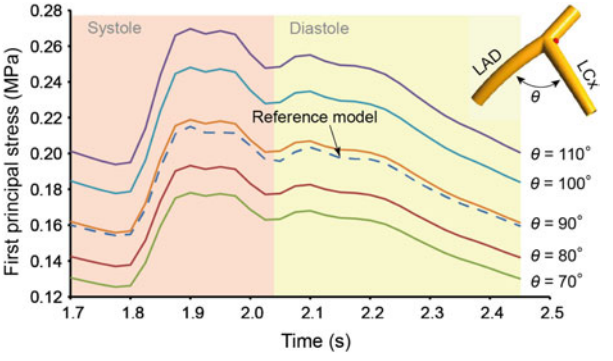

Figure 8. First principal stress at the LCx side bifurcation shoulder.

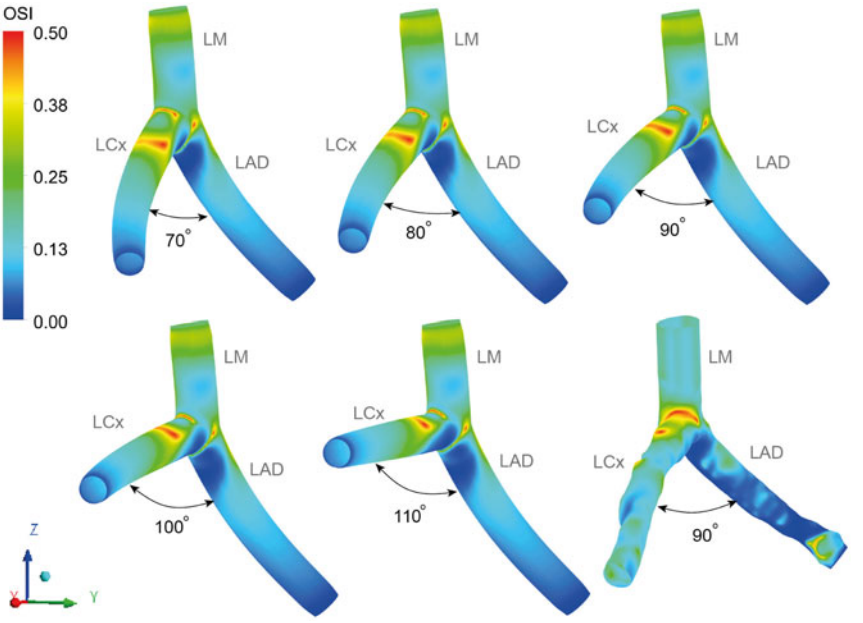

Figure 9. Comparison of OSI distribution for different idealized models.

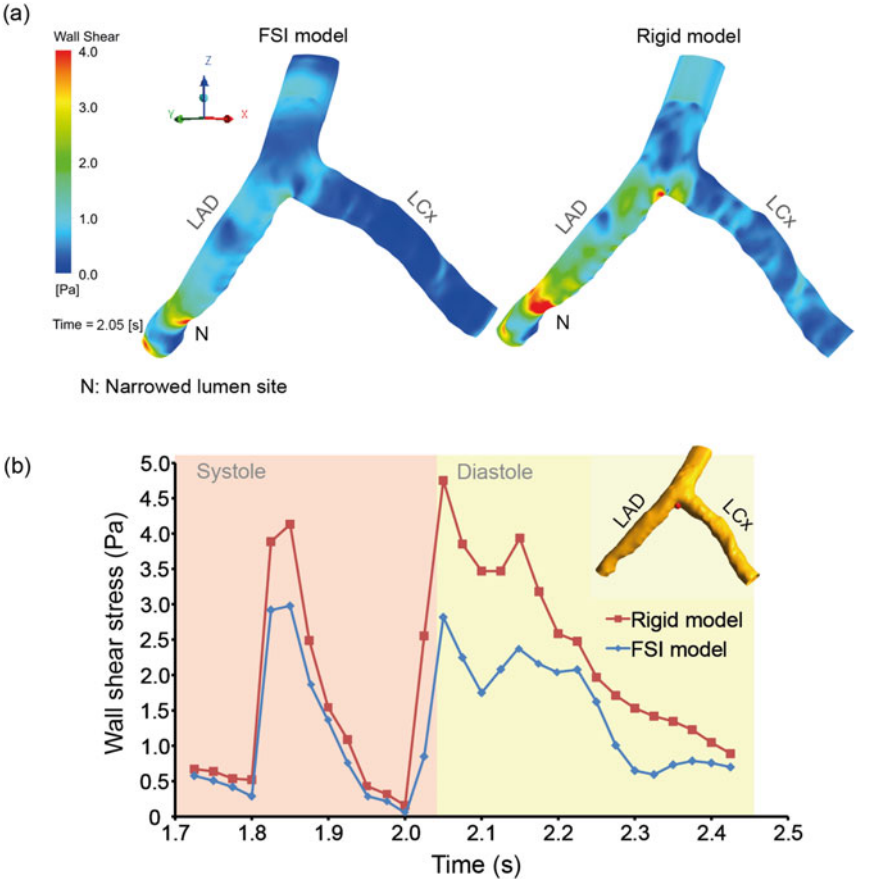

Figure 10. Comparison of FSI and rigid models for the image-based model: (a) WSS distribution at peak diastole ($t = 2.05$ s) and (b) WSS variation over the last cardiac cycle at the bifurcation apex.

WSS and the time-averaged WSS ranging from 0 to 0.5. High OSI indicates unsteady and oscillatory flow with low WSS which leads to a predisposition of endothelial dysfunction and atherogenesis (Ku et al. 1985; Davies 2009; Dong, Inthavong, Tu 2013; Dong, Wong, Tu 2013). Generally, high OSI regions are concentrated at the origins and proximal LCx branches with no significant differences among idealized models. This indicates that the affected regions are susceptible to progress atherosclerotic changes due to the presence of disturbed flow. As a reference, the image-based model shows a similar OSI distribution except in the distal LAD branch, where a locally high OSI is found caused by a moderate bulge section. Due to this luminal expansion, local flow separation and disturbance appear as a result.

WSS results predicted by FSI and rigid model are compared in Figure 10(a). The rigid model predicts a greater distribution of higher WSS values at the peak of diastole phase ($t = 2.05$ s) both at the bifurcation apex and the narrowed lumen site downstream of the LAD branch. In contrast, the FSI model produces lower WSS value at these locations due to considerable vessel expansion driven by the pulsatile blood flow, which is in agreement with the previous studies (Torii, Wood, et al. 2009; Malve et al. 2012). Instantaneous WSS variation at the bifurcation apex is shown in Figure 10(b). At the systole phase, the WSS predicted by the rigid model is slightly larger than the FSI model. However, the WSS magnitude difference becomes greater in the diastole phase. The averaged WSS predicted by the FSI model is smaller than the rigid model by 32%. This significant difference is mainly caused by the increased mass flow rate occurring at the diastole phase than systole. As WSS is proportional to the velocity gradient in the near wall region, and if the arterial wall is assumed to be rigid, then the blood flow will be further accelerated leading to a greater velocity gradient in the near wall region than in an FSI modelling approach.

4. Discussion

The results demonstrate that the variation of branch angle significantly influences the artery mechanical deformation. Wider-angled models cause the LCx side bifurcation shoulder to be continuously exposed under strong first principal stress and high OSI during the whole cardiac cycle.

The first principal stress results of the image-based model show a close agreement with the idealized model ($\theta = 90°$). Therefore, the medical application potential of the proposed FSI coupling method to investigate intravascular flow environment of realistic model is demonstrated.

It is well established that endothelial cells, which form an important part of the vasculature, are involved in promoting an atheroprotective environment by complementary actions of endothelial cell-derived vasoactive factors. Disruption of vascular homoeostasis can lead to the development of endothelial dysfunction, which in turn contributes to the early and late stages of atherosclerosis (Lerman and Zeiher 2005). Endothelial cells experience two major haemodynamic forces *in vivo*: fluid shear stress (τ), which is a frictional force imposed per unit area from blood flow parallel to the vessel wall; and tensile stress (P), which is a normal stretch force resulting from the expansion effect of blood pressure on the vessel (Hahn and Schwartz 2008). Both fluid shear stress and tensile stress play important roles in maintaining the homoeostasis of the blood vessel, but they can also become pathophysiological factors in the complex pathogenesis of atherosclerosis (Chien et al. 1998, Lehoux and Tedgui 1998). For endothelial cells subjected to disturbed flow, endothelial dysfunction occurs when pro-inflammatory phenotype is triggered and developed, and the affected cells are unable to adapt to disturbed flow (Ku et al. 1985; Malek et al. 1999). Therefore, low mean shear stress and marked oscillations in the direction of WSS play critical roles in the development of atherosclerosis.

Vascular smooth muscle cells, serving as the second layer of the vessel from the inner side, appear mainly to respond to tensile stress (Hahn and Schwartz 2008), which is dependent on lumen radius and wall thickness. This stress has been suggested as a main source of mechanical stimuli to promote atherosclerotic plaque formation. Furthermore, it may invoke various signal transductions (i.e. calcium–natrium ion channels, renin–angiotensin systems and integrins) in vascular smooth muscle cells and to stimulate extracellular matrix formation (Osol 1995; Wilson et al. 1995). Accordingly, shear stress and tensile stress are believed to be pathophysiologic stimuli in atherosclerosis (Chatzizisis et al. 2007; Chatzizisis and Giannoglou 2009). Therefore, arterial districts involved by elevated tensile forces and low shear stress environment suggest a high potential of developing atherosclerosis (Thubrikar and Robicsek 1995).

This study provides the insights of the connection between bifurcation angle and the development of coronary atherosclerosis from mechanical and haemodynamics point of view, which differs from angiography assessment conventionally used by clinical study. The clinical study by Sun and Cao (2011) reports that the mean diameter of LCx in patients with a bifurcation angle $\theta > 80°$ was significantly larger than that measured in patients with bifurcation angle $\theta < 80°$ due to the presence of atherosclerotic plaques, and wider bifurcation angles are closely related to the development of atherosclerosis, thus leading to coronary artery disease. Results from this study are consistent with their reports as high tensile stress and low oscillatory WSS simultaneously occur at the LCx side bifurcation shoulder in wider-angled models, a high tendency of inducing atherosclerotic changes is indicated.

Lastly, comparison of numerical results between FSI and rigid models showed not only remarkable qualitative

discrepancies in the WSS distributions over two regions (the bifurcation apex and the moderate narrow lumen site downstream of the LAD branch), but also apparent quantitative differences in the WSS profiles at the bifurcation apex over the diastole phase. Therefore, the effect of the arterial wall compliance on coronary artery haemodynamics plays an important role in the numerical simulation accuracy, and it cannot be neglected for clinical diagnostic purposes (Kabinejadian and Ghista 2012).

Some limitations in this study should be considered. First, no pathological changes such as coronary stenosis are simulated, as the aim of this paper is to investigate the influence of branch angulation changes on coronary haemodynamics, and therefore, the effects of stenosis is not studied in this work. Second, despite the assumption that a Newtonian model is reasonable in coronary artery simulation based on previous studies (Joshi et al. 2004; Gijsen et al. 2007), the approach limits the biological effects of prolonged contact of blood flow with the cells of vascular wall. Third, the angle formed by LM and LAD was set into a constant (Johnston and Kilpatrick 1997) for the purpose of isolating the effect of single geometric factor, while the sequence of angle variation between LAD and LM was neglected. Lastly, due to the lack of patient-specific data and extremely time-consuming model reconstruction procedure, only one CT image-based coronary artery model was selected in this study, and no sub-branches were included during model reconstruction. As mentioned earlier, the numerical predictions compare well with reported clinical studies, and the results of the image-based model are consistent with the idealized model, the reliability of the research findings can be validated.

In conclusion, the branch angulation strongly alters its mechanical stress distribution under pulsatile blood pressure. High tensile and low oscillatory shear stress simultaneously occurs at the LCx side bifurcation shoulder in wider-angled models. Along with the reported clinical findings, a high tendency of inducing atherosclerosis is suggested for the bifurcation shoulder on LCx branch side for wider-angled models. The functional mechanical and haemodynamic indices yielded from this study can facilitate clinicians to have a better understanding of the role of haemodynamics in atherosclerotic disease initiation and progression in the vicinity of bifurcations. Implementations of the proposed research framework over patient-specific models can enable clinicians to non-invasively detect and analyse plaques at early stages, especially in asymptomatic and low-risk patients, which can improve risk stratification without including more invasive procedures.

Funding

The authors acknowledge the financial support provided by the Australian Research Council (ARC project ID DP0986183), and Jingliang Dong especially for the scholarship provided by the China Scholarship Council (CSC Student ID 2010608027) and RMIT University.

Supplemental data

More FSI simulation results of the image-based model as an animation are given in the online supplementary data, which can be accessed at http://dx.doi.org/10.1080/10255842.2014.921682.

References

Boutsianis E, Dave H, Frauenfelder T, Poulikakos D, Wildermuth S, Turina M, Ventikos Y, Zund G. 2004. Computational simulation of intracoronary flow based on real coronary geometry. Eur J Cardio-Thoracic Surg. 26(2):248–256.

Caro CG, Fitz-Gerald JM, Schroter RC. 1969. Arterial wall shear and distribution of early atheroma in man. Nature. 223 (5211):1159–1160.

Caro CG, Fitz-Gerald JM, Schroter RC. 1971. Atheroma and arterial wall shear. Observation, correlation and proposal of a shear dependent mass transfer mechanism for atherogenesis. Proc R Soc Lond B: Biol Sci. 177:109–159.

Cecchi E, Giglioli C, Valente S, Lazzeri C, Gensini GF, Abbate R, Mannini L. 2011. Role of hemodynamic shear stress in cardiovascular disease. Atherosclerosis. 214:249–256.

Chaichana T, Sun Z, Jewkes J. 2011. Computation of hemodynamics in the left coronary artery with variable angulations. J Biomech. 44(10):1869–1878.

Chaichana T, Sun Z, Jewkes J. 2012. Computational fluid dynamics analysis of the effect of plaques in the left coronary artery. Comput Math Methods Med. 2012(2012). doi:10.1155/2012/504367.

Chatzizisis YS, Coskun AU, Jonas M, Edelman ER, Feldman CL, Stone PH. 2007. Role of endothelial shear stress in the natural history of coronary atherosclerosis and vascular remodeling: molecular, cellular, and vascular behavior. J Am Coll Cardiol. 49(25):2379–2393.

Chatzizisis YS, Giannoglou GD. 2009. Myocardial bridges are free from atherosclerosis: overview of the underlying mechanisms. Can J Cardiol. 25(4):219–222.

Chien S, Li S, Shyy YJ. 1998. Effects of mechanical forces on signal transduction and gene expression in endothelial cells. Hypertension. 31:162–169.

Colombo A, Zahedmanesh H, Toner DM, Cahill PA, Lally C. 2010. A method to develop mock arteries suitable for cell seeding and in-vitro cell culture experiments. J Mech Behav Biomed Mater. 3:470–477.

Davies PF. 2009. Hemodynamic shear stress and the endothelium in cardiovascular pathophysiology. Nat Clin Pract Cardiovascular Med. 6(1):16–26.

Dong J, Inthavong K, Tu J. 2013. Image-based computational hemodynamics evaluation of atherosclerotic carotid bifurcation models. Comput Biol Med. 43(10):1353–1362.

Dong J, Wong KKL, Tu J. 2013. Hemodynamics analysis of patient-specific carotid bifurcation: a CFD model of downstream peripheral vascular impedance. Int J Numer Method Biomed Eng. 29(4):476–491.

Gijsen FJ, Wentzel JJ, Thury A, Lamers B, Schuurbiers JC, Serruys PW, van der Steen AF. 2007. A new imaging technique to study 3-D plaque and shear stress distribution in human coronary artery bifurcations *in vivo*. J Biomech. 40 (11):2349–2357.

Girasis C, Serruys PW, Onuma Y, Colombo A, Holmes DR, Jr, Feldman TE, Bass EJ, Leadley K, Dawkins KD, Morice MC. 2010. 3-Dimensional bifurcation angle analysis in patients with

left main disease: a substudy of the SYNTAX trial (SYNergy between percutaneous coronary Intervention with TAXus and cardiac surgery). JACC: Cardiovasc Interv. 3(1):41–48.
Hahn C, Schwartz MA. 2008. The role of cellular adaptation to mechanical forces in atherosclerosis. Arterioscler Thromb Vasc Biol. 28:2101–2107.
Heil M, Hazel AL. 2011. Fluid–structure interaction in internal physiological flows. Annu Rev Fluid Mech. 43:141–162.
Huo Y, Choy JS, Svendsen M, Sinha AK, Kassab GS. 2009. Effects of vessel compliance on flow pattern in porcine epicardial right coronary arterial tree. J Biomech. 42(5):594–602.
Johnston PR, Kilpatrick D. 1997. The effect of branch angle on human coronary artery blood flow. Hobart: International Congress on Modelling and Simulation.
Joshi AK, Leask RL, Myers JG, Ojha M, Butany J, Ethier CR. 2004. Intimal thickness is not associated with wall shear stress patterns in the human right coronary artery. Arterioscler Thromb Vasc Biol. 24(12):2408–2413.
Kabinejadian F, Ghista DN. 2012. Compliant model of a coupled sequential coronary arterial bypass graft: effects of vessel wall elasticity and non-Newtonian rheology on blood flow regime and hemodynamic parameters distribution. Med Eng Phys. 34(7):860–872.
Karner G, Perktold K, Hofer M, Liepsch D. 1999. Flow characteristics in an anatomically realistic compliant carotid artery bifurcation model. Comput Methods Biomech Biomed Eng. 2(3):171–185.
Koshiba N, Ando J, Chen X, Hisada T. 2007. Multiphysics simulation of blood flow and LDL transport in a porohyperelastic arterial wall model. J Biomech Eng. 129 (3):374–385.
Ku DN, Giddens DP, Zarins CK, Glagov S. 1985. Pulsatile flow and atherosclerosis in the human carotid bifurcation. Positive correlation between plaque location and low oscillating shear stress. Arteriosclerosis. 5:293–302.
Lehoux S, Tedgui A. 1998. Signal transduction of mechanical stresses in the vascular wall. Hypertension. 32(2):338–345.
Lerman A, Zeiher AM. 2005. Endothelial function: cardiac events. Circulation. 111:363–368.
Leung JH, Wright AR, Cheshire N, Crane J, Thom SA, Hughes AD, Xu Y. 2006. Fluid structure interaction of patient specific abdominal aortic aneurysms: a comparison with solid stress models. Biomed Eng Online. 5(33). doi:10.1186/1475-925X-5-33.
Malek AM, Alper SL, Izumo S. 1999. Hemodynamic shear stress and its role in atherosclerosis. J Am Med Assoc. 282 (21):2035–2042.
Malve M, Garcia A, Ohayon J, Martinez MA. 2012. Unsteady blood flow and mass transfer of a human left coronary artery bifurcation: FSI vs. CFD. Int Comm Heat Mass Transfer. 39(6):745–751.
Nerem RM, Seed WA. 1983. Coronary artery geometry and its fluid mechanical implications. In: Schettler G, Nerem RM, Schmid-Schönbein H, Mörl H, Diehm C, editors. Fluid dynamics as a localizing factor for atherosclerosis. Berlin, Heidelberg: Springer-Verlag; p. 51–59.
Nichols W, O'Rourke M. 2005. McDonald's blood flow in arteries. London: Hodder Arnold.
Ohayon J, Finet G, Gharib AM, Herzka DA, Tracqui P, Heroux J, Rioufol G, Kotys MS, Elagha A, Pettigrew RI. 2008. Necrotic core thickness and positive arterial remodeling index: emergent biomechanical factors for evaluating the risk of plaque rupture. Am J Physiol-Heart Circ Physiol. 295(2):H717–H727.
Osol G. 1995. Mechanotransduction by vascular smooth muscle. J Vasc Res. 32(5):275–292.
Scotti CM, Shkolnik AD, Muluk SC, Finol EA. 2005. Fluid–structure interaction in abdominal aortic aneurysms: effects of asymmetry and wall thickness. Biomed Eng Online. 4(64). doi:10.1186/1475-925X-4-64.
Slager CJ, Wentzel JJ, Gijsen FJ, Thury A, van der Wal AC, Schaar JA, Serruys PW. 2005. The role of shear stress in the destabilization of vulnerable plaques and related therapeutic implications. Nat Clin Pract Cardiovasc Med. 2(9):456–464.
Soulis JV, Farmakis TM, Giannoglou GD, Louridas GE. 2006. Wall shear stress in normal left coronary artery tree. J Biomech. 39(4):742–749.
Stone PH, Coskun AU, Kinlay S, Popma JJ, Sonka M, Wahle A, Yeghiazarians Y, Maynard C, Kuntz RE, Feldman CL. 2007. Regions of low endothelial shear stress are the sites where coronary plaque progresses and vascular remodelling occurs in humans: an *in vivo* serial study. Eur Heart J. 28 (6):705–710.
Sun Z, Cao Y. 2011. Multislice CT angiography assessment of left coronary artery: correlation between bifurcation angle and dimensions and development of coronary artery disease. Eur J Radiol. 79(2):e90–e95.
Tada S, Tarbell JM. 2005. A computational study of flow in a compliant carotid bifurcation-stress phase angle correlation with shear stress. Ann Biomed Eng. 33(9):1202–1212.
Tang D, Yang C, Kobayashi S, Zheng J, Woodard PK, Teng Z, Billiar K, Bach R, Ku DN. 2009. 3D MRI-based anisotropic FSI models with cyclic bending for human coronary atherosclerotic plaque mechanical analysis. J Biomech Eng. 131(6):061010.
Tezduyar TE, Takizawa K, Brummer T, Chen PR. 2011. Space-time fluid-structure interaction modeling of patient-specific cerebral aneurysms. Int J Numer Methods Biomed Eng. 27:1665–1710.
Thubrikar MJ, Robicsek F. 1995. Pressure-induced arterial wall stress and atherosclerosis. Ann Thorac Surg. 59:1594–1603.
Torii R, Oshima M, Kobayashi T, Takagi K, Tezduyar TE. 2009. Fluid-structure interaction modeling of blood flow and cerebral aneurysm: significance of artery and aneurysm shapes. Comput Methods Appl Mech Eng. 198:3613–3621.
Torii R, Wood NB, Hadjiloizou N, Dowsey AW, Wright AR, Hughes AD, Davies J, Francis DP, Mayet J, Yang GZ, et al. 2009. Fluid–structure interaction analysis of a patient-specific right coronary artery with physiological velocity and pressure waveforms. Commun Numer Methods Eng. 25:565–580.
Vennemann P, Lindken R, Westerweel J. 2007. *In vivo* whole-field blood velocity measurement techniques. Exp Fluids. 42(4):495–511.
Vigmostad SC, Udaykumar HS, Lu J, Chandran KB. 2010. Fluid-structure interaction methods in biological flows with special emphasis on heart valve dynamics. Int J Numer Methods Biomed Eng. 26:435–470.
Wilson E, Sudhir K, Ives HE. 1995. Mechanical strain of rat vascular smooth muscle cells is sensed by specific extracellular matrix/integrin interactions. J Clin Invest. 96(5):2364–2372.
World Health Organization. 2002. The world health report 2002: reducing risks, promoting healthy life. Geneva: World Health Organization.